Supplementary Material for "Emergence of a Chern-insulating state from a semi-Dirac dispersion"

Huaqing Huang,[1,2] Zhirong Liu,[3] Hongbin Zhang,[2] Wenhui Duan,[1,4,5] and David Vanderbilt[2]

[1] *Department of Physics and State Key Laboratory of Low-Dimensional Quantum Physics, Tsinghua University, Beijing 100084, China*
[2] *Department of Physics and Astronomy, Rutgers University, Piscataway, New Jersey 08854-8019, USA*
[3] *College of Chemistry and Molecular Engineering, Peking University, Beijing 100871, China*
[4] *Collaborative Innovation Center of Quantum Matter, Tsinghua University, Beijing 100084, China*
[5] *Institute for Advanced Study, Tsinghua University, Beijing 100084, China*

(Dated: October 4, 2015)

Contents

I. MIRROR SYMMETRY

Rutile TiO_2 is a wide-gap nonmagnetic oxide semiconductor that has been extensively studied experimentally. While VO_2 is a $3d^1$ system, which undergoes a metal-insulator transition near room temperature (340 K in bulk) accompanied by a structural phase transition. As the lattice mismatch between the rutile TiO_2 (a = 4.59 Åand c = 2.96Å) and VO_2 (4.55 and 2.85 Å) is very small, the TiO_2/VO_2 heterostructures and interfaces have received extensive attention and interesting properties have been explored experimentally. For example, a series of superlattices composed of $V_{1-x}W_xO_2$ ($x = 0$ or 0.08) and TiO_2 were fabricated successfully to investigate the interface and carrier-confinement effects of the metal-insulator transition phenomena of VO_2 according to previous work.[1]

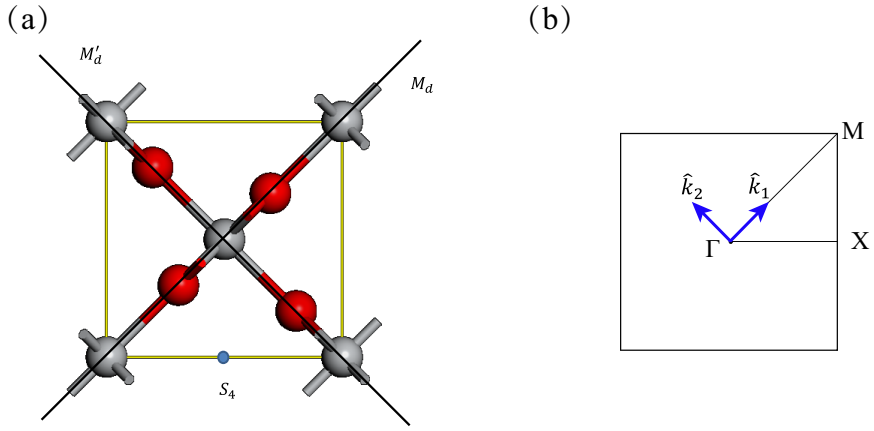

FIG. 1: (a) Schematic illustration of symmetries of the system. (b) High symmetry points in the first Brillouin zone. $\hat{k}_1$ and $\hat{k}_2$ indicate the direction of the new axis.

The multilayer system TiO_2/VO_2 considered in the present work is formed by TiO_2 layers and VO_2 layers grown along the rutile (001) direction. Five layers of TiO2 are more than sufficient to prevent direct interactions between successive VO_2 slabs. The systems are in the space group $P\bar{4}2_1m$ (No.113). The important symmetries of the systems are S_4 and M_d mirror plane (see Fig. 1).

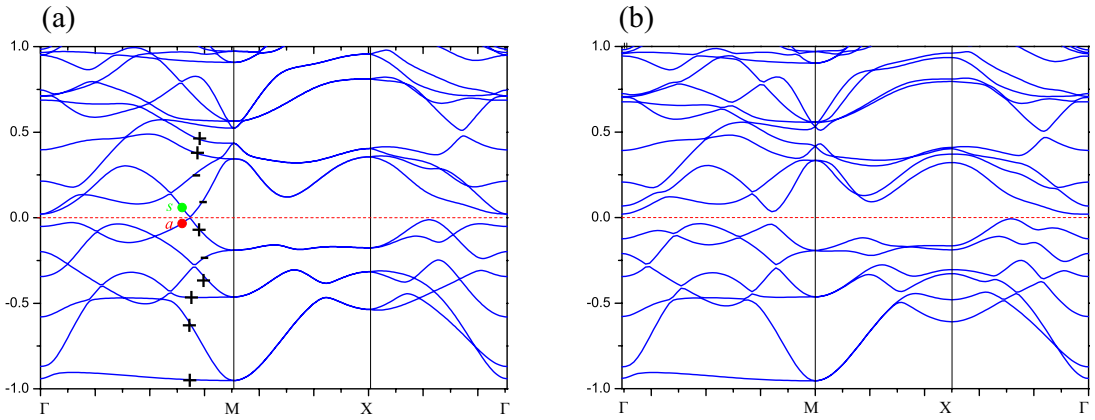

FIG. 2: The spin-up band structures of $(TiO_2)_5/(VO_2)_3$ (a) without external strain and (b) under a shear strain. The "+" and "−" in (a) denote the mirror eigenvalue of the Bloch wavefunction of each band. Spin-orbit coupling (SOC) was excluded in this DFT calculation.

The emergence of the semi-Dirac spectrum without considering spin-orbit coupling, is attributed to the unavoidable band crossing protected by mirror symmetry. The two bands, which cross the Fermi level at single points along the digonals of the first Brillouin zone, belong to different irreps of the mirror symmetry, hence two bands simply cross instead of open a gap when they approach one another at the Fermi level. We label the mirror eigenvalues of several bands near the Fermi level in Fig. 2(a). We also plot the spatial distribution of wavefunctions of the two crossing bands in Fig. 3. The wavefunction is either symmetric or antisymmetric under mirror operation M_d, implying that the states belong to distinct irreps. To further confirm this, we apply a shear strain ($\mathbf{c} \to \mathbf{c} + 0.01\mathbf{a}$) on the superlattice structure to break the mirror symmetry in our first-principles calculation. The results shows that the degenerate point split and a gap of ~ 70 meV opened, indicating that the mirror symmetry is a critical factor for the special electronic structure.

II. TYPE-I AND TYPE-II SEMI-DIRAC MODELS

Since the system have an diagonal mirror symmetry across Γ–M, we then consider effective Hamiltonian based on the M_d symmetry. We first assume that the two bands have the same M_d symmetry, which results out type-I semi-Dirac model. Then we consider the case in the multilayer $(TiO_2)_5/(VO_2)_3$ where two bands have opposite symmetry, which leads to the type-II semi-Dirac model.

A. Two bands have the same M_d symmetry

Firstly, we assume the two bands have the same M_d symmetry. For convenience, herein we define $k_1 = \frac{k_x+k_y}{2}$ ($k_2 = \frac{k_x-k_y}{2}$) for the direction along (perpendicular to) the Γ–M line. For the two crossing bands without SOC, the effective Hamiltonian can be write as, $H = h_x\sigma_x + h_y\sigma_y + h_z\sigma_z$, where $h_i(k_1, k_2)$ are all real function of (k_1, k_2). The generic structure of the Hamiltonian for two bands having the same M_d symmetry is

$$\begin{aligned} h_z(k_1, k_2) &= u(k_1) + v(k_1)k_2^2 + \dots \\ h_x(k_1, k_2) &= s(k_1) + t(k_1)k_2^2 + \dots \end{aligned} \tag{1}$$

and $h_y = 0$, since the Hamiltonian is basically real when SOC is absent. Here we express the $h_{x,y,z}$ in terms of k_2. The M_d symmetry requires both h_x and h_z to be even in k_2, since both bands have the same M_d symmetry. The functions u, v, s and t are just some functions of k_1.

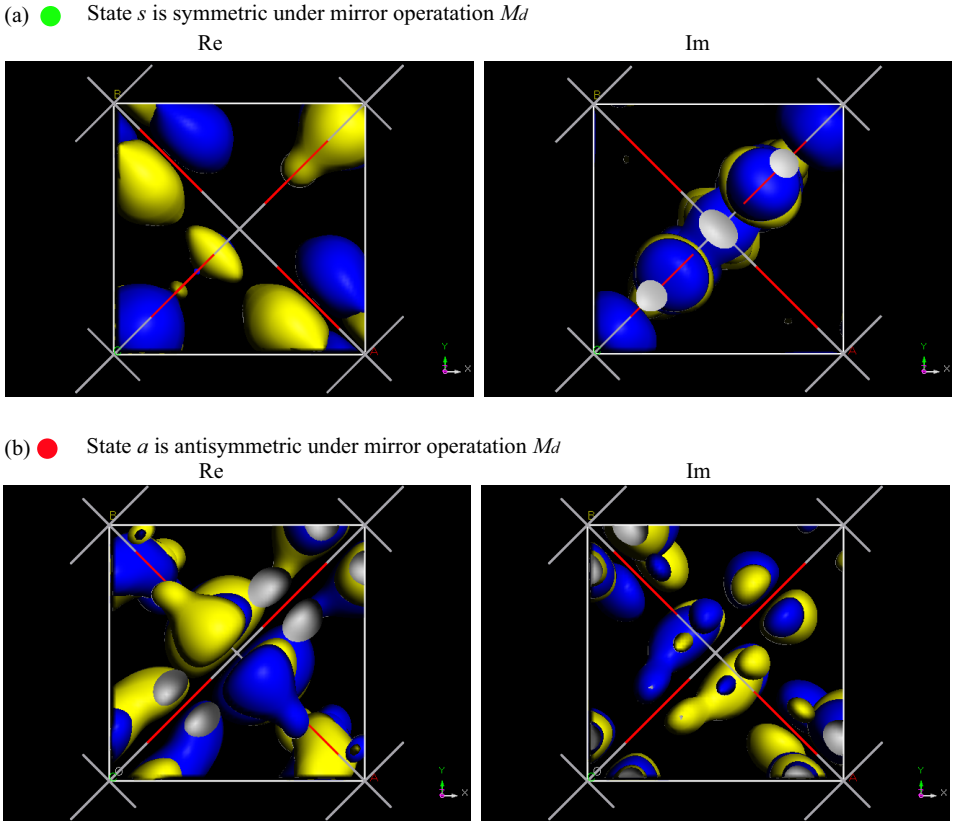

FIG. 3: The isosurface plot of the real and imaginary part of wavefunctions of states s and a [labeled in Fig. 2(a)]. Blue and yellow indicate the opposite signs. State a (s) is antisymmetric (symmetric) under the mirror operation M_d, implying that the two states belong to distinct irreps.

Now it can generically happen that $u(k_1)$ has a zero somewhere along Γ–M; call it $k_1^{(u)}$. Also $s(k_1)$ may have a zero somewhere along Γ–M; call it $k_1^{(s)}$. If and only if $k_1^{(u)} = k_1^{(s)}$ which is not happen generically, we can get a type-I semi-Dirac point.

To be more specific, let's go to relative coordinates. We choose $k_1 = k_1^{(u)}, k_2 = 0$ for reference, and define $q_1 = k_1 - k_1^{(u)}, q_2 = k_2$. Then if we expand the functions near the reference point, we get

$$\begin{aligned} h_z &= Aq_1 + Bq_2^2 + \dots \\ h_x &= C + Dq_1 + Eq_2^2 + \dots \end{aligned} \tag{2}$$

Then we only get a semi-Dirac point along Γ–M (i.e., at $q_2 = 0$) if C=0, which should not happen generically.

If we neglect higher order terms, we can easily find two zero-gap (Dirac) points near the semi-Dirac point: $q_1 = -BC/(BD - AE), q_2 = \pm\sqrt{AC/(BD - AE)}$. By tuning C through zero, the two Dirac points merge into the semi-Dirac point, then disappear with a gap of $2C$ opens. Hence the type-I semi-Dirac model can be viewed as the consequence of the merging of two Dirac points.

More importantly, the Berry curvature should be an odd function of q_2, since both h_x and h_z are even functions of q_2. Hence the integrated Berry curvature would be zero after including the SOC-induced complex hoping term to open a gap, which is inconsistent with the TiO_2/VO_2 system.

B. Two bands have opposite M_d symmetry

Then, we move to the more relevant case of opposite symmetry. According to our above analysis, the two bands that cross the Fermi level along Γ–M line have opposite M_d symmetry, we consider effective Hamiltonian based on

M_d symmetry. The generic structure of the Hamiltonian near the Γ–M line is

$$\begin{aligned} h_z(k_1,k_2) &= u(k_1)+v(k_1)k_2^2+\dots \\ h_x(k_1,k_2) &= s(k_1)k_2+t(k_1)k_2^3+\dots \end{aligned} \tag{3}$$

Since the two bands have opposite M_d symmetry, the bands only couple at odd orders in k_2.

Now let's again define $k_1^{(u)}$ and $k_1^{(s)}$ and go to relative coordinates as before. we choose $k_1 = k_1^{(u)}, k_2 = 0$ for reference, and define $q_1 = k_1 - k_1^{(u)}, q_2 = k_2$. Finally, we get

$$\begin{aligned} h_z &= Aq_1+Bq_2^2+\dots \\ h_x &= Cq_2+Dq_1q_2+\dots \end{aligned} \tag{4}$$

Now we can get a semi-Dirac point if $C = 0$, which only happen when $k_1^{(u)} = k_1^{(s)}$. Keeping only terms up to quadratic order in q_1, q_2 and solving the equations of $h_z = 0, h_x = 0$, we find three zero-gap (Dirac) points near the reference point: $q_1 = q_2 = 0; q_1 = -C/D, q_2 = \pm\sqrt{AC/BD}$. We assume without loss of generality that $A/BD < 0$. With increasing C from negative to positive values, the three Dirac points merge into the semi-Dirac point and then becomes a single Dirac point. This is a type-II semi-Dirac point as we described in the main text.

To make it more clear, we can choose $k_1 = k_1^{(s)}, k_2 = 0$ for reference, and define $q_1 = k_1 - k_1^{(s)}, q_2 = k_2$, we get the expansion

$$\begin{aligned} h_z &= \Delta+Aq_1+Bq_2^2+\dots \\ h_x &= Dq_1q_2+\dots \end{aligned} \tag{5}$$

This is essentially identical to the type-II semi-Dirac model (Eq. (6) in the main text) after an unitary transformation [i.e., a permutation in $\mathbf{h} = (h_x, h_y, h_z)$]. Moreover, Eq. (5) can map onto Eq. (4) by redefining the reference point as $(-C/D, 0)$, so we can identify $C = -\Delta D/A$. Hence, by tuning Δ through zero, we get a generic region with one Dirac point, then the appearance of a semi-Dirac point, then a generic region of three Dirac points. What's more, the integral of Berry curvature is nonzero when considered the SOC interaction, which is consistent with the DFT results of the TiO_2/VO_2 case.

III. MLWF ANALYSIS

In the rutile VO_2 structure, each V ion and the nearest surrounding oxygen ions form a distorted octahedron. Each octahedron shares one edge with adjacent members. Since there are two kinds of VO_6 octahedron whose in-plane O-V-O chain are perpendicular to each other, we use local axis for different V sites. The local z axis is along in-plane O-V-O chain and local y axis is aligned with global c axis [shown in Fig. 1(a) of the main text]. The $3d$ shell of V ions split into doubly degenerate e_g and triply degenerate t_{2g} orbitals due to the octahedral crystal field splitting. Since the local frame defined here is different from ordinary definition in octahedron of perovskite materials, the e_g represents the d_{z^2} and d_{xy} orbitals, while the t_{2g} are d_{xz}, d_{yz} and $d_{x^2-y^2}$ orbitals. Because of the non-regularity (distortion from cubic symmetry) of the VO_6 octahedron, the low lying t_{2g} orbtials of V ions further split into two doubly degenerate $d_\perp$ orbtials (yz and xz) and one $d_\parallel$ orbital (x^2-y^2). Following previous works,[2,3] we label the V atoms as V1, V2, V3 in terms of their distance to the TiO_2 layers.

The nanostructure has a half-metallic electronic structure in the absence of spin-orbit coupling, i.e., electrons of only one spin channel contribute to the metallic bands near the Fermi level, while those of the opposite spin channel form an insulating state. The ferromagnetic configuration of the spins along the rutile c axis is lower in energy than an antiferromagnetic alignment.[2,3] The spin-polarized bands around the Fermi level, which are separated from lower bands by an energy gap, are dominated by the $d_\perp$ and $d_\parallel$ orbitals. We projected the Bloch wavefunction into these local orbitals and get MLWFs, which may serve as ideal building blocks in tight-binding models. As shown in Fig. 1 of the main text, the MLWFs keep the shape and symmetry of local atomic d orbitals. Note that the small lobes at the O sites clearly demonstrate the d-p hybridization, which lead to the splitting of degenerate d states at different V ions.

Duo to the d^1 configuration of V ions in conventional rutile VO_2, the low lying $d_\parallel$ orbital is occupied and dominate the valance bands below the Fermi level, while the unoccupied $d_\perp$ orbitals correspond to the conduction bands. Because the relative energies of the $d_\parallel$ and $d_\perp$ depends upon the c/a ratio which affect the distorted octahedron crystal field splitting,[4] the orbital ordering and occupancies change in the superlattice, which turn out to play an important role for the existence of semi-Dirac cones. In $(TiO_2)_5/(VO_2)_3$ superlattice, the ion position relaxation in the superlattice compress the c/a ratio around V3 layers, hence change the orbital ordering and occupancies. As

TABLE I: On-site energies of t_{2g} orbitals of all V atoms from MLWF calculations.

	d_{xz}	d_{yz}	$d_{x^2-y^2}$
V1	4.67	4.61	3.84
V2	4.68	4.53	3.63
V3	4.82	4.08	4.67

shown in Table I, the on-site energies of d_{yz} is lower than that of $d_{\parallel}$ ($d_{x^2-y^2}$) for V3 atoms, which is different from V1 and V2 atoms. Therefore, V1 and V2 ions have a occupied $d_{\parallel}$, while V3 has a occupied orbital of $d_{\perp}$ of combined d_{xz} and d_{yz} character.

IV. $\mathbf{k}\cdot\mathbf{p}$ ANALYSIS BASED ON FIRST-PRINCIPLES RESULTS

Since the band crossing doesn't happen at high symmetry point such as Γ or M, we conduct the $\mathbf{k}\cdot\mathbf{p}$ analysis numerically to get the effective Hamiltonian in Eq. (7) of the main text. We first solve the MLWF-based TB Hamiltonian H to get all eigenvectors $V = (\mathbf{u}_1, \cdots, \mathbf{u}_n)$ numerically at the band crossing point (k_c, k_c), where $\mathbf{u}_i$ is the eigenvector corresponds to eigenvalue ϵ_i. For convenience, we make a coordinate transformation: $\mathbf{q} = (q_1, q_2) = (k_1 - k_c, k_2) = (\frac{k_x+k_y}{2} - k_c, \frac{k_x-k_y}{2})$. Then we express the Hamiltonian near the the crossing point as

$$H_c(\mathbf{q}) = V^\dagger H V = H_0 + H'(\mathbf{q}) = \begin{pmatrix} A & B \\ B^\dagger & D \end{pmatrix} \tag{6}$$

where $H_0 = \mathrm{diag}(\epsilon_1, \cdots, \epsilon_n)$ is the diagonal matrix which independent with $\mathbf{q}$ and $H'(\mathbf{q})$ is the perturbation term near the band crossing point. Here we suppose A is the 2×2 submatrix that we are interested in (mainly contribute to the two crossing bands). By employing the downfolding method,[5,6] we obtain the 2×2 effective Hamiltonian $H_{\text{eff}} = A + B(\mathrm{E}_F\mathbb{I}_{2\times 2} - D)^{-1}B^\dagger$, where $\mathbb{I}_{2\times 2}$ is the unit matrix and E_F is the Fermi energy. As a lowest order approximation, we adopted $D \approx D_0$, where D_0 is the corresponding part of H_0. Keeping only terms up to quadratic order in $\mathbf{q}$ and performing a unitary transformation to keep the Hamiltonian real-valued, we finally get the $\mathbf{k}\cdot\mathbf{p}$ Hamiltonian

$$H_{\mathbf{k}\cdot\mathbf{p}} = \epsilon(\mathbf{q})\mathbb{I}_{2\times 2} + \mathbf{h}(\mathbf{q})\cdot\vec{\sigma}, \tag{7}$$

with

$$\begin{aligned} \epsilon(\mathbf{q}) &= 3.885 - 0.0792q_1 + 0.2500q_1^2 - 0.06966q_2^2, \\ h_z &= -0.3929q_1 - 0.256q_2^2 - 0.1125q_1^2, \\ h_x &= -0.02044q_2 + 0.1044q_1q_2, \\ h_y &= 0. \end{aligned} \tag{8}$$

Clearly, the Hamiltonian satisfies the above symmetry analysis of Sec. II B. To make a direct comparison with the type-II semi-Dirac model given in the main text, we rotate the $\mathbf{h}(\mathbf{q}) = (h_x, h_y, h_z)$ to $\mathbf{h}'(\mathbf{q}) = (h'_x, h'_y, h'_z) = (-h_z, h_x, 0)$ using a unitary transformation.

It is worth noting that the Hamiltonian is not an effective model in the whole Brillouin zone but only well-defined near the crossing point. As shown in Fig. 4, $H_{\mathbf{k}\cdot\mathbf{p}}$ describes the band structure near the crossing point well. Furthermore, after adding a small terms in h_y to open a band gap at the crossing point, we found that the model provide a Berry flux of $\Phi \approx -\pi$. What's more, the Berry curvature near the crossing point is of banana-shape as shown in Fig. 5, which entirely corresponds with the DFT results in Fig. 2(c) of the main text.

Note that there is a small linear term of q_2 in $H_{\mathbf{k}\cdot\mathbf{p}}$ which should vanish for an exact semi-Dirac spectrum. This term is not forbidden by symmetry, therefore it is generally expected to be present. From the above symmetry analysis, we know that the semi-Dirac spectrum can easily depart from the transition point [$C = 0$ in Eq. (4)]. Hence we expect that this term should exist in general and can be tuned by external strain or other perturbation.

However, $H_{\mathbf{k}\cdot\mathbf{p}}$ indeed belongs to the type-II semi-Dirac model which can provide a nonzero Berry flux. By solving the equations of $\mathbf{h}(\mathbf{q}) = 0$, we find three zero-gap (Dirac) points near the origin in the complex $\mathbf{q}$-space: $q_1 = q_2 = 0$ and $(q_1, q_2) = (0.1957 \mp 0.0002045i, 0.0005742 \pm 0.5628i)$ (in units of a^{-1}, where a is the in-plane lattice constant). If we gradually decrease the linear term of q_2 to zero, three Dirac points move and merge at $\mathbf{q} = (0, 0)$, as exactly

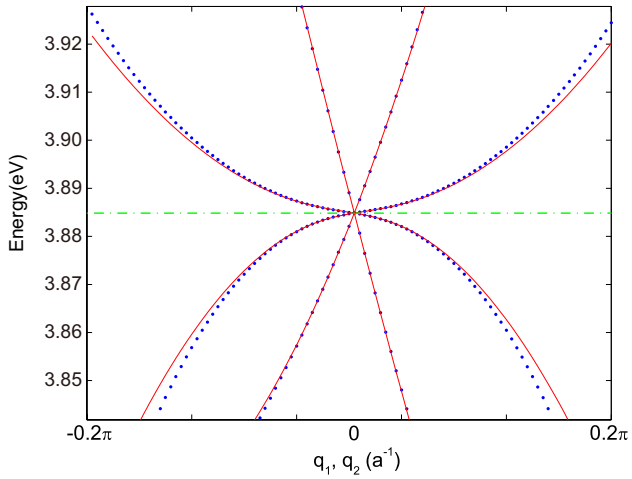

FIG. 4: Band structures along q_1 and q_2 near the crossing point. Blue dots and red lines represent results from MLWF-based TB Hamiltonian H and $H_{\mathbf{k}\cdot\mathbf{p}}$ respectively.

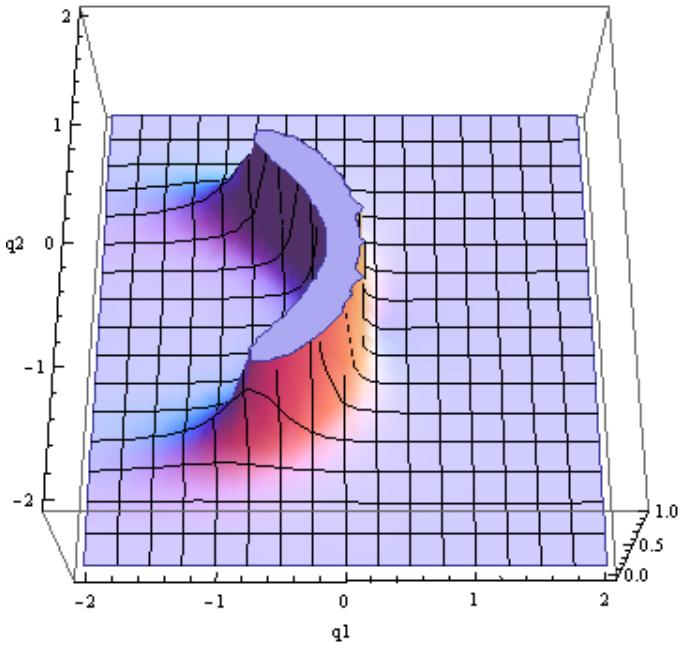

FIG. 5: Calculated Berry curvature $-\Omega$ from $H_{\mathbf{k}\cdot\mathbf{p}}$ after including the SOC-induced h_y term to open a gap at the crossing point.

predicted by the type-II semi-Dirac model. Hence, we conclude that the $\mathbf{k}\cdot\mathbf{p}$ Hamiltonian belongs to the type-II semi-Dirac model. Moreover, the calculated band structure, banana-shaped Berry curvature and nonzero Berry flux indicate that the $H_{\mathbf{k}\cdot\mathbf{p}}$ Hamiltonian, even though is not exactly at the transition point of the type-II semi-Dirac model, should be very close to it. Therefore, we conclude that the TiO_2/VO_2 nanostructure is a Chern insulator and its low-energy electronic structure can be described by a type-II semi-Dirac model.

[1] K. Shibuya, M. Kawasaki, and Y. Tokura, Phys. Rev. B **82**, 205118 (2010).
[2] V. Pardo and W. E. Pickett, Phys. Rev. Lett. **102**, 166803 (2009).
[3] V. Pardo and W. E. Pickett, Phys. Rev. B **81**, 035111 (2010).

[4] J. B. Goodenough, J. Solid State Chem. **3**, 490 (1971).
[5] I. V. Solovyev, Z. V. Pchelkina, and V. I. Anisimov, Phys. Rev. B **75**, 045110 (2007).
[6] H. Huang, W. Duan, and Z. Liu, New J. Phys. **15**, 023004 (2013).